Monthly Notices of the ROYAL ASTRONOMICAL SOCIETY
MNRAS **450,** 1846–1855 (2015) doi:10.1093/mnras/stv688

Spectroscopic detections of C III] λ1909 Å at $z \simeq 6$–7: a new probe of early star-forming galaxies and cosmic reionization

Daniel P. Stark,[1⋆] Johan Richard,[2] Stéphane Charlot,[3] Benjamin Clément,[1,2] Richard Ellis,[4] Brian Siana,[5] Brant Robertson,[1] Matthew Schenker,[4] Julia Gutkin[3] and Aida Wofford[3]

[1]*Steward Observatory, University of Arizona, 933 N Cherry Ave, Tucson, AZ 85721, USA*
[2]*Centre de Recherche Astrophysique de Lyon, Universite Lyon 1, 9 Avenue Charles Andre, F-69561 Saint Genis Laval Cedex, France*
[3]*UPMC-CNRS, UMR7095, Institut d'Astrophysique de Paris, F-75014 Paris, France*
[4]*Cahill Center for Astronomy & Astrophysics, California Institute of Technology, Pasadena, CA 91105, USA*
[5]*Department of Physics & Astronomy, University of California, Riverside, CA 92507, USA*

Accepted 2015 March 26. Received 2015 March 24; in original form 2014 August 15

ABSTRACT

Deep spectroscopic observations of $z \gtrsim 6.5$ galaxies have revealed a marked decline with increasing redshift in the detectability of Ly α emission. While this may offer valuable insight into the end of the reionization process, it presents a challenge to the detailed spectroscopic study of bright photometrically-selected distant sources now being found via deep *Hubble Space Telescope* imaging, and particularly those highly magnified sources viewed through foreground lensing clusters. In this paper, we demonstrate the validity of a new way forward via the detection of an alternative diagnostic line, C III] λ1909 Å, seen in spectroscopic exposures of a star-forming galaxy at $z_{\rm Ly\alpha} = 6.029$. We also report tentative detection of C III] λ1909 Å in a galaxy at $z_{\rm Ly\alpha} = 7.213$. The former 3.3σ detection is based on a 3.5 h XShooter spectrum of a bright ($J_{125} = 25.2$) gravitationally-lensed galaxy behind the cluster Abell 383. The latter 2.8σ detection is based on a 4.2 h MOSFIRE spectra of one of the most distant spectroscopically confirmed galaxies, GN-108036, with $J_{140} = 25.2$. Both targets were chosen for their continuum brightness and previously-known redshift (based on Ly α), ensuring that any C III] emission would be located in a favourable portion of the near-infrared sky spectrum. Since the availability of secure Ly α redshifts significantly narrows the wavelength range where C III] is sought, this increases confidence in these, otherwise, low-signal-to-noise ratio detections. We compare our C III] and Ly α equivalent widths in the context of those found at $z \simeq 2$ from earlier work and discuss the motivation for using lines other than Ly α to study galaxies in the reionization era.

Key words: galaxies: evolution – galaxies: formation – galaxies: high-redshift – cosmology: observations.

1 INTRODUCTION

In the last few years, *Hubble Space Telescope* (*HST*) imaging has delivered several hundred galaxies with photometric redshifts estimated to be above $z \simeq 7$ (e.g. Ellis et al. 2013; McLure et al. 2013; Schenker et al. 2013a; Bouwens et al. 2015). Yet concerted efforts to secure spectroscopic redshifts through the detection of Ly α emission have led to minimal progress. At the time of writing there are fewer than 10 spectroscopically-confirmed galaxies beyond $z \simeq 7$ (Vanzella et al. 2011; Ono et al. 2012; Schenker et al. 2012; Finkelstein et al. 2013; Schenker et al. 2014), and no convincing example beyond $z = 7.62$. While this represents some progress compared to 2006 when the frontier was at redshift 6.96 (Iye et al. 2006), the investment of telescope time to push the frontier back a mere 100 Myr in look-back time has been very costly. The relevant spectroscopic campaigns probing beyond $z \simeq 7$ have achieved a success rate for Ly α significantly lower than at $z \simeq$ 5–6, where large equivalent width Ly α emission is found in more than half of the galaxies observed (Stark et al. 2010, 2011). The most natural explanation for the downturn in Ly α transmission in similarly-selected star-forming galaxies is that the intergalactic

⋆ E-mail: dpstark@email.arizona.edu

medium (IGM) is still partially neutral at $z \simeq 7$, causing attenuation of Ly α (e.g. Treu et al. 2013; Schenker et al. 2014).

While the reduced transmission of Ly α at $z \gtrsim 7$ provides valuable insight into the end of the reionization process, it also has profound implications for future spectroscopic studies of galaxies within the reionization era. The arrival of efficient near-infrared spectrographs (McLean et al. 2012) and the discovery of a growing number of bright gravitationally-lensed galaxies (e.g. Richard et al. 2011; Zitrin et al. 2012; Bradley et al. 2014) promises great progress not only in measuring redshifts but also in spectroscopic diagnostic studies of typical early galaxies. However, with Ly α increasingly obscured, presumably by the partially-neutral IGM at $z > 7$, the current approach of targeting Ly α is unlikely to be productive. Indeed, even a 52 h exposure recently undertaken with the ESO VLT failed to detect the line in a promising bright $z \simeq 7$ target (Vanzella et al. 2014).

The disappointing outcome of earlier spectroscopic efforts raises several important strategic questions. If Ly α is undetectable in most star-forming galaxies in the reionization era, must we rely entirely on photometric redshifts and imaging data to determine their physical properties? In fact, if there are no detectable features in the rest-frame UV, it would be unclear whether ground-based telescopes, including more powerful ones soon under construction, can contribute much to the study of early galaxies. Moreover, while *JWST* will ultimately provide access to strong nebular emission lines ([O III] λ5007, Hα) to $z \sim 8$, spectroscopic studies at the highest redshifts ($z > 11$–15), where new sources are likely to be found, must perforce rely on detectable rest-frame UV features.

Ly α is usually considered to be the only prominent UV emission line for star-forming galaxies. But this perception is mostly based on spectroscopic studies of relatively massive, chemically-enriched galaxies undergoing fairly rapid ($\gtrsim$10 $M_\odot$ yr^{-1}) star formation (e.g. Shapley et al. 2003). However, the galaxies that populate the reionization era are likely to have lower masses, reduced metallicities and larger specific star formation rates (SFR). In an important, in-depth, study of a metal-poor (1/6 $Z_\odot$) galaxy at $z \sim 2$, Erb et al. (2010) demonstrated the presence of numerous prominent emission lines (O III] $\lambda\lambda$1661,1666; He II λ1640, and the blended C III] λ1908 Å doublet) throughout the rest-frame UV spectral region. Additional low-mass galaxies have recently shown similar rest-UV emission spectra (Christensen et al. 2012; Bayliss et al. 2014; James et al. 2014).

In an attempt to select galaxies with physical properties similar to those expected in the reionization era, Stark et al. (2014) secured deep rest-frame UV spectra for 17 faint gravitationally-lensed galaxies at $z \simeq 1.5$–3 with characteristic very blue UV colours ($<\beta> \simeq -2.2$) and intrinsic (unlensed) stellar masses ranging from 2×10^6 to 1.4×10^9 $M_\odot$. In this campaign, the C III] λ1908 Å doublet was typically the strongest line other than Ly α and detected in 16 galaxies with rest-frame equivalent widths up to 14 Å. Stark et al. (2014) interpreted such powerful metal line emission as arising from the large ionization parameters and electron temperatures associated with metal-poor galaxies dominated by very young stellar populations. While the UV metal lines will never have equivalent widths as large as Ly α (which can reach above 120 Å), they will not be affected by the neutral hydrogen in the IGM.

Thus, based on the emerging picture at $z \simeq 2$, the strongest UV metal lines (C IV λ1549, O III] $\lambda\lambda$1661,1666, C III] λ1908 Å) may offer a promising route to securing redshifts and illuminating the physical nature of a subset of bright star-forming galaxies in the reionization era. Stark et al. (2014) predicted that existing ground-based facilities should be able to detect these UV metal emission lines in the brightest ($H < 25.5$) $z \gtrsim 6$ galaxies. In this paper, we present the first results from an ongoing campaign targeting UV metal line emission in the spectra of $z \gtrsim 6$ galaxies. In the initial phase of this programme, our primary goal has been to verify that metal line equivalent widths are similar to those seen in metal poor $z \simeq 2$ galaxies. To maximize the likelihood of success, we have chosen targets that have bright continuum magnitudes ($H \lesssim 25.5$) and known (Ly α-based) spectroscopic redshifts. The latter requirement ensures that the relevant metal emission lines would lie in regions where the atmospheric transmission is near unity and obscuration from sky emission lines minimal. Clearly in the longer term, it is desirable to demonstrate spectroscopic detections for bright systems where Ly α is completely suppressed.

Here we report VLT/XShooter and Keck/MOSFIRE spectroscopic observations of the C III] λ1908 doublet in two $z > 6$ galaxies. The first system we discuss is a bright gravitationally-lensed system at $z = 6.03$. The galaxy, reported in Richard et al. (2011) and Bradley et al. (2014), is multiply-imaged into a pair by the foreground cluster Abell 383. The two images, A383-5.1 and A383-5.2, are both bright (J_{125}=24.6 and 25.2) and highly-magnified (11.4 $\times$ and 7.3 $\times$). Ly α emission was detected in each image by Richard et al. (2011) and, at the redshift $z_{\mathrm{Ly}\alpha} = 6.029$, the C III] doublet falls within a relatively clean region of the J band. The second system we discuss is GN-108036, a $z = 7.2$ galaxy located in the GOODS North field. This galaxy was first identified as a bright ($J_{140} = 25.2$) z-band dropout in Ouchi et al. (2009). Ly α emission was reported in Ono et al. (2012), providing spectroscopic confirmation at $z_{\mathrm{Ly}\alpha} = 7.213$. At this redshift, the C III] doublet is located in a region free from atmospheric absorption within the H band.

The paper is organized as follows. We discuss our new near-infrared spectroscopic observations and reduction procedures in Section 2. The properties of Ly α and C III] for both sources are detailed in Section 3. We describe the modelling of the continuum and emission lines for A383-5.2 in Section 4. By determining the velocity offset of Ly α with respect to C III] we discuss the implications for the interpretation of the evolution of the fraction of photometrically-selected galaxies with Ly α emission in Section 5. Finally, we discuss the prospects of using C III] in future surveys and summarize our conclusions in Section 6. Throughout the paper, we adopt a Λ-dominated, flat Universe with $\Omega_\Lambda = 0.7$, $\Omega_M = 0.3$ and $H_0 = 70\,h_{70}$ km s^{-1} Mpc^{-1}. All magnitudes in this paper are quoted in the AB system (Oke & Gunn 1983).

2 OBSERVATIONS AND DATA REDUCTION

2.1 VLT/XShooter

As part of ESO programme ID: 092.A-0630 (PI: Richard), the galaxy A383-5.2 (Richard et al. 2011) was observed with the XShooter spectrograph on the VLT (Vernet et al. 2011). We chose to pursue A383-5.2 because A383-5.1 (the brighter of the two lensed images) is located closer to the cluster centre, where diffuse light from bright cluster galaxies contributes considerably to the background in the near-infrared. Observations were conducted on the nights of 2013 October 27 and December 15 for 3 and 2 observing blocks (OBs) of 1 h each, respectively. We used the 11 arcsec $\times$ 0.9 arcsec slit oriented to avoid bright galaxies (Fig. 1). One OB comprised three exposures of 955 s in the visible arm, covering the wavelength range 5630–10 090 Å at a resolution of $R \sim 8800$, and three exposures of 968 s in the near-infrared arm (with four sub-integrations of 242 s), covering the wavelength range 10 350–24 780 Å at a resolution of $R \sim 5300$. A dither pattern of $\pm$2.5 arcsec

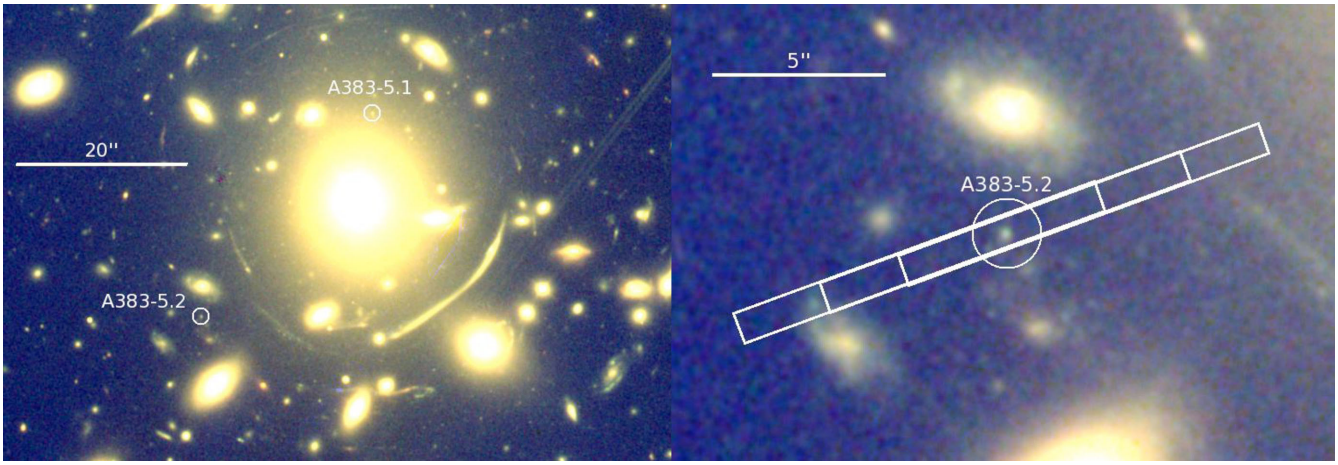

Figure 1. Overview of the VLT/XShooter observations of the $z_{Ly\alpha} = 6.027$ galaxy A383-5.2 first reported in Richard et al. (2011). Left: location of the targeted image A383-5.2 with respect to the cluster centre. Right: position and orientation of the XShooter slit, showing the three dither positions.

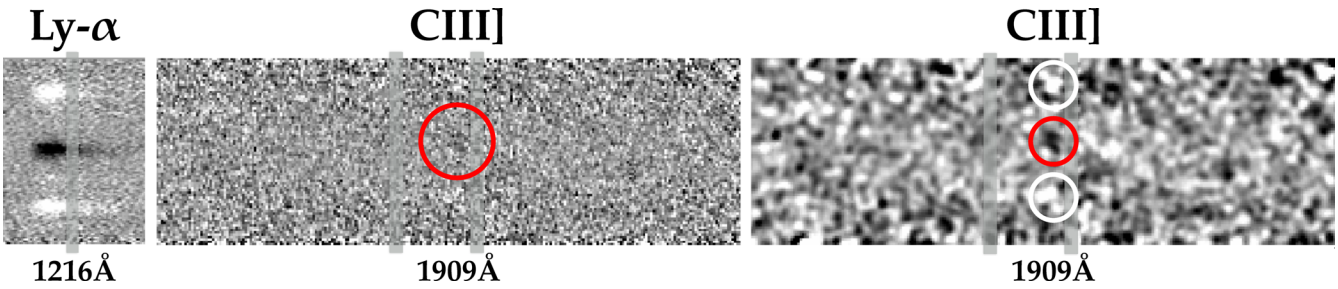

Figure 2. XShooter 2D spectrum of the $z_{Ly\alpha} = 6.027$ galaxy A383-5.2. The leftmost panel is centred on Ly α emission which is detected with the visible arm at 0.8546 μm. The location of C III] λ1909 at 1.3412 μm is shown in the middle (unsmoothed) and rightmost (smoothed) panels. The smoothing is performed via a Gaussian filter with radius of 3 pixels. The [C III] λ1907 emission line is under the OH sky line just bluewards of C III] λ1909.

along the slit was performed between each exposure, for optimal sky subtraction (Fig. 1, right). The total exposure time on source was 14 325 s in the visible arm and 14 520 s in the near-infrared arm.

The sky conditions were clear and the seeing was very good in the first three OBs, with a range of 0.50–0.70 arcsec and a median seeing of 0.55 arcsec, but less good in the second set of two OBs, with a range of 0.60–0.90 arcsec. A spectroscopic standard star was observed on both nights for absolute flux calibration, and multiple telluric standard stars were observed to estimate telluric correction.

We used the latest version of the XShooter data reduction software (v.2.2.0) in the Recipe Flexible Execution Workbench (REFLEX) environment to perform a first calibration and reduction of each exposure. We then applied standard IDL and IRAF routines for optimally combining and extracting the 15 exposures. Specifically, we used the Lyman α emission line, well detected in each exposure, to correct for variations in seeing and atmospheric conditions between the different OBs, and applied a scaling and weighting of the 2D spectra according to the flux and detection level of the Lyman α line. We also used the spatial position of the line measured in the reduced spectrum to precisely compute the offsets between each OB for optimal combination. We used the same offsets, scaling factors and weights to combine the exposures in the near-infrared arm. Applying these corrections slightly strengthened the signal-to-noise ratio (S/N) of the C III] line, increasing our confidence in the detection.

The combined 2D spectrum was extracted using a variance-weighting scheme in IRAF based on the detected profile of the lines. We also used the normalized extracted spectrum of the telluric standards to apply a median correction for telluric absorptions in the near-infrared arm. The final combined 2D spectrum at wavelengths near Ly α and C III] are presented in Fig. 2 and discussed in Section 3.1

2.2 Keck/MOSFIRE

We secured spectroscopic observations of GN-108036 with MOSFIRE (McLean et al. 2012) on the Keck I telescope on the nights of 2014 March 6 and April 11. GN-108036 is one of the most distant spectroscopically-confirmed galaxies at $z = 7.213$, first verified by Ono et al. (2012) based on three separate exposures with the DEep Imaging Multi-Object Spectrograph (DEIMOS) on Keck II; the rest-frame equivalent width of Ly α is reported as 33 Å. During the March run, we compiled a total of 3.1 h of exposure in the *H* band with a 0.8 arcsec slit. Conditions were generally clear, but with slight cloud during the first half of the observations. The median full width at half-maximum (FWHM) of a reference star included on the mask was 0.6 arcsec. On the April night, we secured an additional 1.1 h, with a median seeing FWHM of 0.5 arcsec and clear conditions.

The data were reduced using the regular MOSFIRE data reduction pipeline (DRP)[1] following a procedure similar to that described in Schenker et al. (2014) to which the reader is referred. Briefly, this

[1] https://code.google.com/p/mosfire/

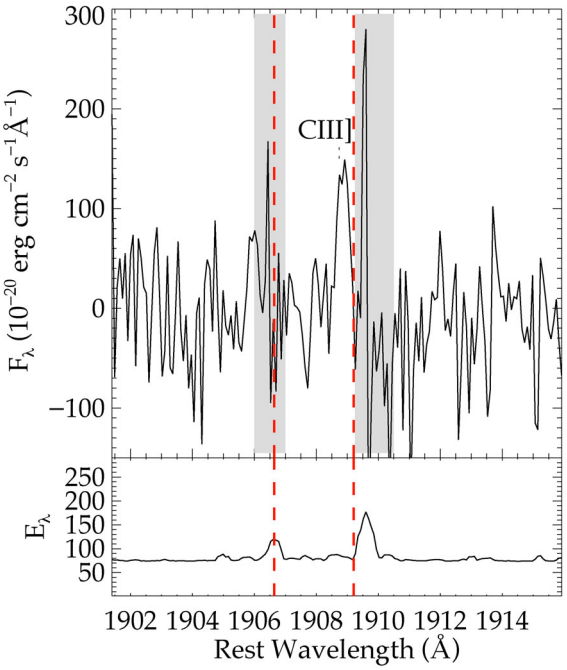

Figure 3. Extracted 1D XShooter spectrum of the spectroscopically-confirmed $z = 6.027$ galaxy A383-5.2. The likely C III] emission feature is noted with a dotted line in the top panel. Red dashed lines denote the narrow window over which C III] is expected based off of the Ly α redshift. The measured line flux of the 3.3σ detection is 3.7×10^{-18} erg cm^{-2} s^{-1}. Wavelengths of strong skylines are visible in the error spectrum shown in the bottom panel. Units of the error spectrum are identical to the object spectrum.

pipeline first creates a median, cosmic ray subtracted flat-field image for each mask. Wavelength solutions for each slit are fit interactively for the central pixel in each slit, then propagated outwards to the slit edges to derive a full wavelength grid. Background subtraction is handled as a two-stage procedure. First, individual stacks of all A frames and all B frames are used to produce A-B and B-A stacks. As the A and B frames are temporally interleaved, this provides a first level of subtraction. Secondly, a 2D b-spline model is fit to the residuals in each of these stacks. The two stacks are then shifted, rectified and combined, producing a positive source signal flanked by two negative signals at approximately half strength, separated by the dither length. To account for the variation in conditions during the March run, we split the data into three segments of $\simeq$1 h each, which were then run through the DRP separately. To produce a final science stack, the resulting three images plus the single reduced image from our April data were then stacked using inverse-variance weighting. The final stack has an average 5σ flux limit of 1.8×10^{-18} erg cm^{-2} s^{-1} in between sky lines, consistent with the expectation produced from the MOSFIRE exposure time calculator. The final combined 2D spectrum at a wavelength near C III] is presented in Fig. 3 and discussed in Section 3.2 below.

3 REST-UV SPECTROSCOPIC PROPERTIES

3.1 A383-5.2

3.1.1 Large equivalent width Ly α emission

The Ly α emission line of both A383-5.1 and A383-5.2 was first reported in the original Richard et al. (2011) paper following observations with the DEIMOS spectrograph on the Keck II telescope. In the discovery spectrum, Ly α was significantly detected (S/N = 7.3), but it was blended with a sky line and the slit was slightly offset from the target (Richard, private communication), precluding reliable constraints on the line strength and profile.

Fig. 2 demonstrates a much more significant detection of Ly α. The improved spectral resolution of XShooter separates Ly α from the nearby sky line. We derive a total Ly α line flux of 1.2×10^{-16} erg cm^{-2} s^{-1}. Correcting for slit losses (taking into account the size of the galaxy, the slit width, and the seeing), we estimate an aperture correction of 1.06. The peak of the line occurs at 8545.6 Å, implying a Ly α redshift of $z_{\mathrm{Ly}\alpha} = 6.0294$. After correcting for the source magnification (7.3 × ; Richard et al. 2011) and applying the aperture correction, the total Ly α luminosity is 6.8×10^{42} erg s^{-1}.

The Ly α equivalent width is inferred via two different methods. First, using the measured line flux and the upper limit (2σ) on the continuum flux from the XShooter spectrum ($<4.8 \times 10^{-19}$ erg cm^{-2} s^{-1} Å^{-1}), we derive a lower limit on the rest-frame equivalent width ($W_{\mathrm{Ly}\alpha,0} > 83$ Å). Since the continuum is usually well below spectroscopic flux limits, it is common to use the continuum flux measured from broad-band imaging to calculate the equivalent widths of emission lines. With this second method, we infer $W_{\mathrm{Ly}\alpha,0} = 138$ Å, consistent with the upper limit derived above and placing A383-5.2 among the most extreme Ly α emitters at $z \simeq 6$ (e.g. Ouchi et al. 2010; Pentericci et al. 2011; Stark, Ellis & Ouchi 2011; Curtis-Lake et al. 2012). The large equivalent width likely reflects both a larger-than-average escape fraction of Ly α radiation ($f_{\mathrm{esc,Ly}\alpha}$) and an efficient production rate of Ly α photons (as might be expected for a young metal-poor system). Assuming a metallicity of 0.2 $Z_\odot$, a Chabrier IMF, and 10 per cent ionizing photon escape fraction) and using Bruzual & Charlot (2003) stellar population models, the Ly α luminosity of A383-5.2 implies an SFR of 3.2 $(f_{\mathrm{esc,Ly}\alpha})^{-1}$ $M_\odot$ yr^{-1}.

3.1.2 C III] λ1909 emission

At $z \simeq$ 2–3, the C III] equivalent width generally increases with the Ly α equivalent width (e.g. Shapley et al. 2003; Stark et al. 2014). For Ly α emitters with equivalent widths as large as A383-5.2 ($W_{\mathrm{Ly}\alpha,0} = 138$ Å), the blended C III] λ1908 doublet would be expected to have a rest-frame equivalent width above 10 Å. However at $z \gtrsim 6$ the resolution of XShooter resolves the C III] doublet, so each of the individual components will be detected with somewhat lower equivalent widths. Given the bright apparent magnitude of A383-5.2 ($J_{125} = 25.2$), both components of C III] should be above the XShooter detection limits if located in between the OH sky lines.

Knowledge of the spectroscopic redshift from Ly α allows us to estimate the observed wavelengths of C III]. However, a precise determination must account for the fact that the peak of the emergent Ly α profile is typically offset with respect to the systemic redshift probed by C III]. For low-mass star-forming galaxies similar to A383-5.2, the centroid of the blended C III] doublet is blueshifted between 60 and 450 km s^{-1} (with a mean of 320 km s^{-1}) from Ly α (Stark et al. 2014). We thus expect [C III] λ1907 to lie between 1.3383 and 1.3400 μm and C III] λ1909 to lie between 1.3397 and 1.3415 μm, each of these windows spanning just 30 spectral pixels. Since the spatial position is also well established (by the location of Ly α along the slit), the window over which we expect to see C III] is confined to a very small area in the spectrum.

Examination of the XShooter spectrum reveals a 3.3σ emission feature at 1.3412 μm, in the spectral window expected for the C III] λ1909 emission line (Fig. 2). The feature is in the centre of the slit at the spatial location of A383-5.2 and is blueshifted by 120 km s^{-1} with respect to Ly α, implying a C III] λ1909 redshift of $z = 6.0265$ (Fig. 3). At this redshift, [C III] λ1907 is unfortunately coincident with an atmospheric OH line at 1.3397 μm. There is a positive emission feature at the expected location, but the noise associated with the sky line precludes useful flux constraints. The flux of C III] λ1909 is $3.7 \pm 1.1 \times 10^{-18}$ erg cm^{-2} s^{-1}. As we will show below, the chance of randomly finding a 3.3σ fluctuation in the small 30 pixel area defined by Ly α is very small.

To compare the UV spectrum of A383-5.2 to that of UV line emitters at $z \simeq 2$–3 (e.g. Erb et al. 2010; James et al. 2014; Stark et al. 2014), we must estimate the flux in the [C III] λ1907 line. The ratio of the individual components of C III] is set by the electron density. Over the range of gas densities typical in high-redshift star-forming galaxies (10^2 and 10^4 cm^{-3}; e.g. Hainline et al. 2009; James et al. 2014), the [C III] λ1907/C III] λ1909 ratio varies between 1.6 and 1.2, respectively. Taking the ratio as 1.4 ± 0.2, we estimate that the total flux in the C III] doublet is $8.9 \pm 2.7 \times 10^{-18}$ erg cm^{-2} s^{-1}. Via the same procedure we described for Ly α (and applying an aperture correction of 1.06×), we determine the total rest-frame C III] equivalent width to be 22.5 ± 7.1 Å.

Confidence in the detection is bolstered by two tests. As described above, prior knowledge of the redshift allows us to define a very small (30 pixel) search window for each component of the C III] doublet. The likelihood of randomly finding a 3.3σ emission feature in the area expected for C III] is highly unlikely. In $N = 10^5$ realizations of the error spectrum, the probability of randomly seeing the observed feature in the 30 pixel window is just 0.25 per cent. We have also verified that the emission feature is not dominated by spurious emission in 1 or 2 of the 15 exposures. We visually examined each of the exposures and verified that hot pixels and cosmic rays are not present. We also split the exposures into two subsets. The first group contains the six exposures with the best seeing and stable conditions (as defined by the Ly α detection in the visible arm), and the second group contains the nine frames over which the seeing degraded. The C III] emission feature is 2.5 × more significant in the stack with the best seeing, as would be expected if the line is associated with A383-5.2 and not a detector artefact. While the C III] λ1907 feature is somewhat close to a sky line, it is cleanly separated by two resolution elements. We do not find other instances of 3.3σ residuals appearing at this separation from sky lines in the XShooter spectrum.

3.2 GN-108036

The centroid of Ly α (0.9984 μm) reported for GN-108036 by Ono et al. (2012) places C III] in the *H* band. Assuming the velocity offset of Ly α with respect to C III] is between 0 and 450 km s^{-1} (e.g. Stark et al. 2014), [C III] λ1907 will be located between 1.563 59 and 1.565 94 μm and C III] λ1909 between 1.565 28 and 1.567 63 μm. With the spectral resolution of MOSFIRE, each window spans only 14 spectral pixels. Fig. 4 reveals a faint emission feature in the small window as expected for C III] λ1909. The 1D extraction is shown in Fig. 5. Clearly the feature is not as prominent as in A383-5.2 (Fig. 2) but this is perhaps not surprising given the lower Ly α equivalent width (33 Å). The line is in a region free from skyline contamination, and the centroid is consistent with the expected position of the target along the slit to within 3 pixels, or 0.55 arcsec. We measure a flux of $0.9 \pm 0.3 \times 10^{-18}$ erg cm^{-2} s^{-1} in an aperture of 1.1 arcsec in the spatial direction and 13 Å in the spectral direction. With a S/N of 2.8, it is difficult to reliably determine the line centroid. Positive emission roughly spans 1.5672–1.5684 μm. If the emission shown in Fig. 4 is C III] λ1909, it would imply a small velocity offset for Ly α (between −150 and 76 km s^{-1}), consistent with Ly α emerging near the systemic redshift. At the redshift of GN-108036, the two components of the C III] doublet are split by 17 Å. For the C III]

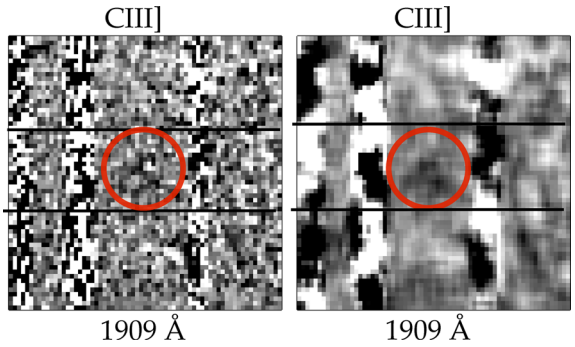

Figure 4. MOSFIRE 2D *H*-band spectrum of the $z = 7.213$ galaxy GN-108036 (unsmoothed in the left-hand panel, smoothed in the right-hand panel). The spectroscopic redshift from Ono et al. (2012) allows the spectrum to be converted to the rest-frame. Black horizontal lines define the location of the galaxy on the MOSFIRE slit. The red circle denotes the expected wavelength and spatial position of the C III] λ1909 emission line. The flanking negative signals resulting from the A–B dither pattern and subtraction are seen above and below the red circle. Smoothing is conducted with a boxcar average with width of 4 pixels.

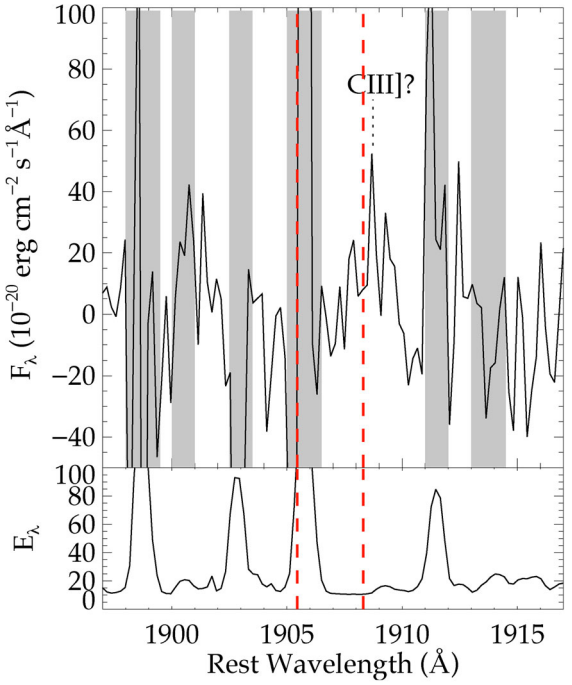

Figure 5. Extracted MOSFIRE 1D spectrum of GN-108036. The tentative 2.8σ C III] emission feature is marked by a dotted line. The error spectrum is shown in the bottom panel with the same units as the object spectrum in the top panel. Red dashed lines denote the narrow window over which the centroid C III] is expected based off of the Ly α redshift. Sky emission features are apparent in the error spectrum and are denoted in the top panel by vertical grey swath. The integrated line flux is 0.9×10^{-18} erg cm^{-2} s^{-1}. Deeper data are ultimately required to verify the tentative detection.

λ1909 redshift defined by the emission feature described above, the [C III] λ1907 line would lie underneath the bright OH skyline visible bluewards of the C III] λ1909 in Fig. 3. The noise is more than 3 × larger on the skyline, precluding identification of the second component.

One test of the reality of the detection is to measure the fluxes at the expected positions of the two negative images flanking the emission feature. As our final stack is the sum of an A–B image and a shifted B–A image, we expect two negative images, each of approximately half the total flux, offset above and below the positive image by the dither length of 2.5 arcsec. We find that this is the case and measure significances of 2.0σ above the line, and 1.9σ below. We further evaluate the line in the four separate subsets of the data discussed earlier, each with an exposure time of ≃1 h. In each subset, we measure a positive S/N in the same aperture used to measure the composite line flux.

To compute the total equivalent width of the less secure C III] detection, we follow the same procedure we described in Section 3.1.2. Given the likely range of electron densities (10^2 cm^{-3}–10^4 cm^{-3}), we expect a [C III] λ1907/C III] λ1909 flux ratio of 1.4 ± 0.2. Taking into account the uncertainty in the flux ratio and the noise in the C III] λ1909 flux, we estimate a [C III] λ1907 flux of 1.3 ± 0.5 × 10^{-18} erg cm^{-2} s^{-1}. The C III] doublet rest-frame equivalent width implied by this analysis (7.6 ± 2.8 Å) is lower than seen in A383-5.2, but is consistent with the Ly α–C III] equivalent width relationship for $z \simeq 2$–3 galaxies from Stark et al. (2014).

Although the detection of C III] λ1909 is much less secure than that of A353-5.2, it is a good indication of the challenge and prospects of securing non-Ly α redshifts for typical $z > 7$ sources. Deeper MOSFIRE data with exposure times in excess of 6–8 h may be required for convincing measurements of the fluxes and equivalent widths of such examples. Given the lower significance of the C III] λ1909 detection in GN-108036, we will focus most of the remaining discussion on the more secure detection in A383-5.2.

4 MODELLING THE CONTINUUM AND EMISSION LINES OF A383-5.2

The broad-band SED of A383-5.2 (Fig. 6) exhibits a very strong break between the H_{160} band and the [3.6] and [4.5] bands. Richard et al. (2011) interpret this as a Balmer break indicative of an evolved (800 Myr) stellar population. Alternatively, the break could arise if nebular emission from [O III]+H β and H α provide substantial contributions within the [3.6] and [4.5] filters, as might be expected if the SED is dominated by a very young stellar population. Distinguishing between these two very different interpretations of the SED is clearly important and can only proceed via direct measurements of the rest-frame optical emission lines. Here we consider whether adding a C III] line flux constraint, which is sensitive to star formation on shorter time-scales than that based on the stellar continuum, can clarify the past star formation history of A383-5.2.

4.1 Method

We fit the continuum spectral energy distribution (SED) and C III] equivalent width of A383-5.2 using an approach similar to that adopted in Stark et al. (2014). We use the latest version of the Bruzual & Charlot (2003) stellar population synthesis model with the standard photoionization code CLOUDY (Ferland et al. 2013) to describe both the stellar and gaseous emission (Gutkin et al., in preparation, who follow the prescription of Charlot & Longhetti 2001).

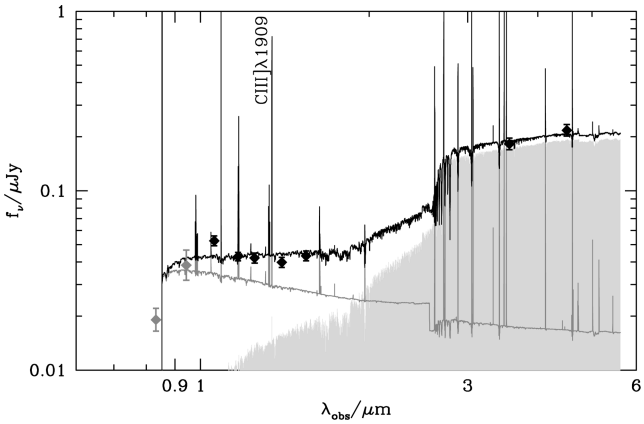

Figure 6. SED of A383-5.2 and population synthesis models which provide best fit to the continuum SED and C III] equivalent width. The observed SED is denoted by the diamond data points. The two grey data points at <1 μm are not included in the fit because of the uncertainty associated with Ly α emission contamination and IGM absorption. The data are best fit by a model with a two component star formation history. The UV continuum and C III] equivalent width are powered by a recent star formation episode (grey curve), while the optical continuum is dominated by an older generation of stars (solid grey swath). The composite SED is shown in black.

Further details are provided in Stark et al. (2014) but, in brief, the main parameters of the photoionized gas are its interstellar metallicity, Z, the typical ionization parameter of a newly ionized H II region, U (which characterises the ratio of ionizing photon to gas densities at the edge of the Strömgren sphere) and the dust-to-metal (mass) ratio, ξ_d (which characterizes the depletion of metals on to dust grains). We consider models with C/O (and N/O) abundance ratios ranging from 1.0 to 0.05 times the standard values in nearby galaxies [$(C/O)_\odot \approx 0.39$ and $(N/O)_\odot \approx 0.09$] to describe the delayed release of C and N by intermediate-mass stars relative to shorter lived massive stars in young galaxies. We also include attenuation of line and continuum photons by dust in the neutral ISM, using the two-component model of Charlot & Fall (2000), as implemented by da Cunha, Charlot & Elbaz (2008, their equations 1–4). This is parametrized in terms of the total V-band attenuation optical depth of the dust, $\hat{\tau}_V$, and the fraction μ of this arising from dust in the diffuse ISM rather than in giant molecular clouds. Accounting for these two dust components is important in differentiating the attenuation of emission-line and stellar continuum photons.

As we will describe in more detail in Section 4.2, the need to simultaneously fit the continuum SED and the C III] equivalent width motivates us to explore a wider range of star formation histories than Stark et al. (2014). In particular, we consider models with two-component star formation histories: a 'starburst' component (represented by a 10-Myr-old stellar population with constant SFR) and an 'old' component (represented by a stellar population with constant or exponentially declining SFR with age between 10 Myr and the age of the Universe at the galaxy redshift). We adopt the same stellar metallicity for both components matching that of the gas phase. The relative contribution of the burst component is a free parameter; in the limiting case where the burst provides a negligible contribution to the stellar mass fraction, the star formation history approaches the single-component star formation histories which are commonly used in high-redshift SED fitting. Given the young ages at redshifts $z > 6$, this simple modelling of star formation and chemical enrichment adequately samples the allowed

Table 1. Results of fitting procedure for A383-5.2. Details are provided in Section 4.1, and results are discussed in Section 4.2.

Model fit to A383.5.2	
$\log U$	$-1.79^{+0.36}_{-0.43}$
$\log(M_{*,\rm young}/M_{*,\rm tot})$	$-2.99^{+0.05}_{-0.03}$
$\log(Z/Z_{\odot})$	$-1.37^{+0.23}_{-0.16}$
$\log(\rm C/O)$	$-0.57^{+0.06}_{-0.06}$
$\log(\rm age/yr)$	$8.72^{+0.10}_{-0.10}$
$\log(M_{*,\rm tot}/\rm M_{\odot})$	$9.50^{+0.10}_{-0.10}$
$\log(\rm SFR/M_{\odot}yr^{-1})$	$0.30^{+0.07}_{-0.07}$
$\hat{\tau}_V$	$0.05^{+0.05}_{-0.05}$

parameter space. We adopt a Chabrier (2003) initial mass function in all models.

To interpret the combined stellar and nebular emission from A383-5.2, we build a comprehensive grid of models covering wide ranges of input parameters. Specifically, we take about 70 model ages between 10 Myr and the age of the Universe (at the redshift of the galaxy we are modelling) for the old stellar component; 30 stellar mass fractions of the starburst relative to the old components, spaced logarithmically between 10^{-3} and unity; metallicities $Z = 0.0001$, 0.0002, 0.0005, 0.001, 0.002, 0.004, 0.008, 0.017 and 0.03; gas ionization parameters $\log U = -1.0$, -1.5, -2.0, -2.5, -3.0, -3.5 and -4.0; dust-to-metal ratios $\xi_{\rm d} = 0.1$, 0.3 and 0.5; C/O (and N/O) scaling factors 1.0, 0.85, 0.65, 0.45, 0.25, 0.15 and 0.05; 10 attenuation optical depths $\hat{\tau}_V$ between 0 and 1; and, for each $\hat{\tau}_V$, two values of μ (0.3 and 0.9). We adopt a Bayesian approach similar to that of Pacifici et al. (2012, their equation 2.10) to compute the likelihood of each model given the data.

4.2 A383-5.2

The acceptable parameter fits are shown in Table 1. Including the nebular line constraints in the modelling has provided several key advances. First, the dependence of emission-line equivalent widths on the ionized gas physical conditions allows new constraints on the metallicity, relative C/O abundance and ionization parameter in star-forming galaxies at $z \simeq 6$. As can be seen in Table 1, the large equivalent width of C III] in A383-5.2 requires models with a very low metallicity ($\log Z = -1.33^{+0.27}_{-0.20}$), large ionization parameter ($\log U = -1.79^{+0.36}_{-0.43}$), and low C/O ratio ($\log \rm C/O = -0.57^{+0.06}_{-0.06}$), similar to the population of ultrafaint lensed galaxies at $z \simeq 2$ (Stark et al. 2014). These constraints are almost entirely lost when the C III] equivalent width is not included in the fitting procedure. The total stellar mass implied by the models is 3.2×10^9 $\rm M_{\odot}$, in close agreement with that reported in Richard et al. (2011). The current SFR is 2.0 $\rm M_{\odot}$ $\rm yr^{-1}$. This estimate is within two times that inferred from the Ly α luminosity in Section 3.1.1. Given the systematic uncertainties in both quantities and the slightly different model assumptions, we consider this agreement satisfactory.

We find that single-component star formation histories struggle to reproduce the continuum SED and C III] equivalent width. Very young ($\lesssim 10^7$ yr), dusty, and metal poor models can reproduce the apparent Balmer Break with strong [O III]+H β and H α emission dominating the [3.6] and [4.5] fluxes. But with strong attenuation and substantial reddening, the young single component models underpredict the C III] equivalent width and overestimate the H_{160} flux. Similarly, while an old stellar population produced by a single-component star formation history can account for the large break between the H_{160} band and [3.6], it is unable to reproduce a large equivalent width C III] emission or a blue UV continuum slope supported by the available imaging and spectroscopy.

We thus find that the observational data indicate a two-component star formation history (Fig. 6). The nebular lines and far-UV continuum are dominated by a recent burst, while the rest-optical light seen by the *Spitzer*/IRAC filters is powered by a somewhat older stellar population. Both populations contribute roughly equally to the emerging near-UV continuum. The young burst component contributes very little to the total stellar mass ($\sim 10^{-3}$) but provides enough ionizing output to match the observed C III] equivalent width.

A383-5.2 is certainly not unique in this respect at very high redshift: Rodríguez Espinosa et al. (2014) have recently argued that a two-component star formation history is necessary to explain the combined emission-line and continuum constraints on a pair of galaxies at $z = 5.07$. But whether multicomponent star formation histories are typical among at $z \gtrsim 6$ sources is not yet clear. Very young stellar ages (<10 Myr for constant star formation) have been suggested based on the large equivalent width of optical nebular emission lines required to match the *Spitzer*/IRAC colours of $z \simeq$ 7–8 galaxies (e.g. Finkelstein et al. 2013; Smit et al. 2014). But it is unlikely that such systems (located 650–800 Myr after the big bang) have only been forming stars for such a short period. Indeed, the average stellar continuum of $z \simeq 8$ galaxies is indicative of older (100 Myr for constant star formation) stars (Dunlop et al. 2013; Labbé et al. 2013). Multicomponent star formation histories with a recent upturn powering the nebular emission provide a natural explanation for this tension. As larger samples of galaxies with UV metal line and high S/N continuum constraints emerge, it will be possible to clarify the nature of early galaxy star formation histories in more detail.

5 REIONIZATION AND THE LYα VELOCITY OFFSET

The attenuation of Ly α emission from galaxies at $z \gtrsim 6$ provides a valuable probe of reionization. Ground-based spectroscopy has been used by several groups to measure the redshift-dependent fraction of UV selected galaxies at $z \gtrsim 6$ with Ly α emission (e.g. Stark et al. 2010; Ono et al. 2012; Schenker et al. 2012). As described in Section 1, the Ly α emitter fraction appears to drop rapidly over $6 < z < 8$ (e.g. Fontana et al. 2010; Caruana et al. 2012, 2014; Ono et al. 2012; Treu et al. 2013; Pentericci et al. 2014; Schenker et al. 2014; Tilvi et al. 2014), as might be expected if the IGM is partially neutral at $z \simeq$ 7–8.

Theoretical efforts are now focused on determining how neutral the IGM must be at $z \simeq$ 7–8 in order to reproduce the drop in visibility of Ly α emission beyond $z \simeq 6$. During the late stages of reionization, the cosmic H II regions surrounding star-forming galaxies are expected to be very large. As a result, the impact of IGM damping wing absorption on Ly α emission is likely to be minimal in the final phase of reionization when neutral hydrogen fractions are low. Because of this, most attempts to model the drop in the Ly α emitter fraction require that the IGM evolves from being fully ionized at $z \simeq 6$ to a neutral fraction by volume as large as 60 per cent at $z \simeq 7$ (e.g. McQuinn et al. 2007; Mesinger & Furlanetto 2008; Jensen et al. 2013).

Such a striking evolution in the ionization state of the IGM seems unphysical over such a brief period of cosmic history (e.g. Robertson et al. 2013; Mesinger et al. 2015; Sobacchi & Mesinger

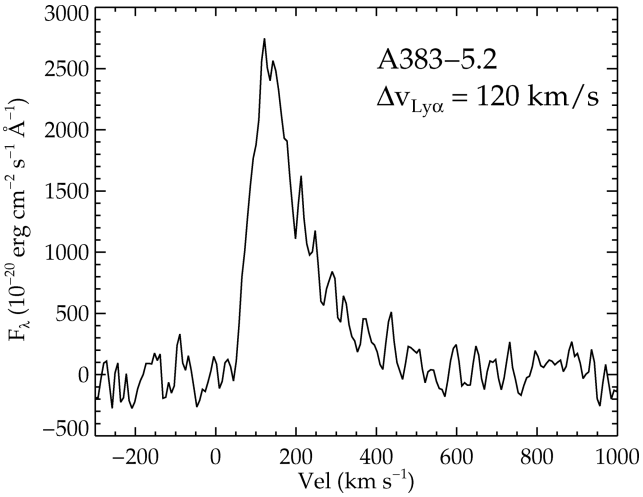

Figure 7. Velocity profile of Ly α emission in the $z = 6.027$ galaxy A383-5.2. Ly α is shifted to the rest frame using the systemic redshift provided by C III] λ1909. The peak flux of Ly α emission is shifted by $\Delta v = 120$ km s^{-1} from the systemic redshift.

2014). As a result, alternative explanations have been considered. If the photoionizing background drops at $z \gtrsim 6$, the prevalence of self-shielded systems within ionized regions of the IGM would increase rapidly, providing an additional source of opacity for Ly α photons (Bolton & Haehnelt 2013). Furthermore, if the escape fraction of ionizing radiation (f_{esc}) increases by a small amount over $6 < z < 7$ ($\Delta f_{esc} = 0.1$), the Ly α luminosity may be significantly reduced (Dijkstra et al. 2014). Finally, if the velocity offset between Ly α and the galaxy systemic redshift is less than observed at low redshift, a partially neutral IGM would be more effective at attenuating Ly α, thereby lowering the neutral fraction required to reproduce the observations (e.g. Dijkstra, Mesinger & Wyithe 2011; Schenker et al. 2014; Mesinger et al. 2015).

Of the three factors described above, the Ly α velocity offset is the most feasible to constrain via direct observations. If the Ly α velocity offset is similar to that found in bright UV-selected galaxies at $z \simeq 2$ ($\Delta v_{Ly\alpha} = 445$ km s^{-1}; Steidel et al. 2010), the IGM would likely have to be mostly neutral at $z \simeq 7$ to be consistent with the Ly α observations at the 1σ level (Mesinger et al. 2015). But if the Ly α velocity offset is lower (i.e. $\Delta v_{Ly\alpha}$ 200 km s^{-1}) as is often seen in strong Ly α emitters (e.g. Tapken et al. 2007; McLinden et al. 2011; Hashimoto et al. 2013), the downturn in Ly α visibility could be produced with an IGM that is still substantially ionized ($Q_{H\,II} \lesssim 0.6$; Mesinger et al. 2015) at $z \simeq 7$. Schenker et al. (2013b) already indicated a possible reduction in the velocity offset with increasing redshift by comparing observations of [O III] and Ly α in UV-selected galaxies at $z \simeq 3.5$ with similar samples at $z \simeq 2$. Albeit with a small sample of nine sources, their velocity offsets were typically $\simeq$150 km s^{-1}.

However, at $z \gtrsim 4$, such rest-frame optical emission lines are not detectable from the ground. Thus, since the UV metal lines probe the galaxy systemic redshift (e.g. Erb et al. 2010; Stark et al. 2014), they provide the only immediate means of determining the distribution of $\Delta v_{Ly\alpha}$ at $z \simeq 6$. Indeed, the likely detection of C III] λ1909 in A383-5.2 would provide the first constraint on the Ly α velocity offset in a $z \gtrsim 5$ galaxy, revealing an offset of only 120 km s^{-1} (Fig. 7). Such a low Ly α velocity offset is consistent with an extension of the redshift-dependent trend found in Schenker et al. (2013b), likely reflecting the general increase in the Ly α equivalent width over $3 < z < 6$ seen for similarly selected UV sources (Stark et al. 2011).

The less secure detection of C III] λ1909 in Fig. 5, although not as significant as that in A383-5.2, may imply that the Ly α offset of GN-108056 is even smaller. Deeper data are required to verify the detection and accurately measure the line centroid. While A383-5.2 is observed when the Universe is highly ionized, GN-108056 is likely observed in a partially neutral IGM. At $z \gtrsim 7$, the IGM damping wing absorption will attenuate Ly α most strongly in systems with low-velocity offsets. Focusing our UV metal line follow-up on galaxies with known Ly α detections should bias us towards galaxies with significant transmission through the surrounding IGM. In principle, this should cause us to select the subset of Ly α emitters with large velocity offsets. The fact that we find little to no velocity offset for GN-108036, one of the few known Ly α emitters at $z \simeq 7$, might reflect the absence of large velocity offsets in the reionization era.

If small Ly α velocity offsets are common at $z \gtrsim 6$, the IGM evolution required to reproduce the downturn in the Ly α fraction would be less rapid than previous estimates using large Ly α velocity offsets, providing a more physically reasonable reionization history (see Robertson et al. 2010, 2013; Mesinger et al. 2015). As the number of bright $z \gtrsim 6$ galaxies with Ly α detections increases, it will be feasible to assemble a moderate sample of $z \simeq 6$ galaxies with Ly α and UV metal line detections, providing the first measurement of the distribution of Ly α velocity offsets in reionization-era galaxies and thereby removing one of the key systematic uncertainties in mapping Ly α evolution to a reionization history.

6 DISCUSSION AND SUMMARY

Considerable effort has been placed in spectroscopic study of $z \gtrsim 6$ galaxies. Yet, in spite of significant allocations of telescope time to several research teams, few spectroscopic redshifts have been confirmed beyond $z \simeq 7$ due to the absence of Ly α. Although the physical explanation for this suppression is of interest in its own right in terms of constraining the reionization history, it is essential to locate lines other than Ly α in distant sources for many reasons. First, the Ly α emitter fraction test is currently applied to a photometrically selected sample. If no line is detected, there is an obvious ambiguity in interpretation between a suppressed Ly α at the redshift of interest and a foreground object. Clearly securing the redshift from an additional line breaks this degeneracy. Secondly, as discussed in Section 5, the interpretation of the redshift-dependent Ly α fraction in terms of the evolving neutral fraction depends on the velocity offset of the line with respect to the systemic redshift which, at $z > 6$, can only be determined with current facilities using rest-frame UV nebular lines. Finally, Stark et al. (2014) demonstrate, via detailed modelling, how measures of rest-frame UV lines such as N IV], O III], C IV, Si III] and C III] can provide unique information on important physical properties of galaxies during the reionization era, including the ionization parameters, metallicities and star formation histories which remain degenerate when interpreting SEDs based on broad-band photometry alone.

In this paper, we have demonstrated it may be feasible to detect the C III] 1908 Å doublet in the growing sample of bright ($H \simeq 25$) star-forming galaxies at $z > 6$. The two sources we discuss are very different and illustrate the challenges even with state-of-the-art near-infrared spectrographs on the largest ground-based telescopes. A363-5.2 is a gravitationally lensed galaxy at a redshift $z_{Ly\alpha} = 6.029$. It is bright ($J_{125} = 25.2$), highly magnified ($\times$7.4) and a likely 3.3σ C III] λ1909 detection has been secured

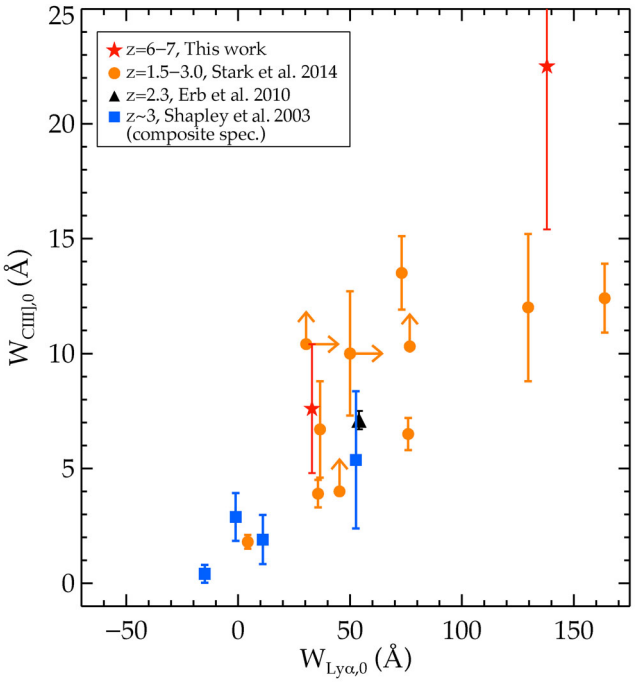

Figure 8. A comparison of the rest-frame equivalent widths of C III] 1909 Å and Ly α from the study of $z \simeq 2$ lensed sources by Stark et al. (2014, orange points), Erb et al. (2010) and the $z \simeq 3$ Shapley et al. (2003) composite alongside the two new C III] detections beyond $z \simeq 6$ (this paper, red stars).

in only a 3.5 h exposure. The source is typical of the brightest sources that have been located in lensing surveys of foreground clusters (e.g. the CLASH programme). GN-108036 is more typical of the bright sources found in deep blank field surveys. Although not fainter ($J_{140} = 25.2$), as it is unlensed, it is more luminous and even with a 4.2 h exposure, the putative C III] feature is much fainter and only detected at 2.8σ. Clearly deeper data are highly desirable to confirm this detection.

The likely detection of C III] in A383-5.2 has enabled us to measure a reduced velocity offset of Ly α in a $z > 6$ source as well as to break degeneracies of interpretation in the SED. Specifically, including the strength of C III] in our modelling fits to the SED allows us to determine a low metallicity ($\log Z = -1.37$), a large ionization parameter ($\log U = -1.79$) and a low C/O ratio. More importantly, however, we argue the tension between the strength of C III] (which is sensitive to star formation on 10 Myr time-scales) and the measured Balmer break and rest-frame UV continuum slope (indicative of a more mature population) can be reconciled if the star formation has been erratic with a recent burst of activity contributing significantly to the nebular spectrum. If this behaviour is typical of $z > 6$ star-forming galaxies, it may explain the prominent rest-frame optical nebular lines inferred in recent studies (e.g. Smit et al. 2014).

As discussed in Section 1, a long-term goal for future ground-based facilities would be a redshift survey based on rest-frame UV lines other than Ly α, particularly in securing more precise measures of the Ly α fraction. However, we have considered it is prudent in the first instance to base our searches using those few targets for which Ly α has already been detected. This may, admittedly, lead to some biases in interpretation if, for example, the sources have untypical Ly α fluxes for some reason. As one progresses to higher redshift, the flux ratio of C III] to Ly α should increase since Ly α is increasingly suppressed and C III] is more prominent in metal-poor systems. Fig. 8 gives no strong evidence of a shift in this direction compared to the distribution seen at lower redshift by Stark et al. (2014) but the samples are small and uncertainties remain large.

It should be emphasized that the claimed C III] detections reported here were only possible for bright, spectroscopically confirmed galaxies. It will be much more challenging for current facilities to locate such metal lines in a blind manner for similar and fainter sources where the redshifts are not a priori known, (e.g. from Ly α detections) given that OH sky lines and gaps in atmospheric transmission can obscure emission features.

Fortunately, imaging surveys continue to deliver bright photometric candidates likely at $z \gtrsim 6$. Many of these are gravitationally lensed systems located behind lensing clusters (e.g. Bradley et al. 2014; Smit et al. 2014), while others are from blank-field surveys with *HST* (e.g. Smit et al. 2015 and ground-based cameras (Bowler et al. 2014). We have demonstrated in this paper that modest exposures with current facilities can reach the necessary limits to detect metal lines if they have equivalent widths of $\simeq$10 Å, similar to comparable systems at $z \simeq 2$. Despite the observational challenges, we argue that such work will be of great value in guiding future programmes with JWST and 20–40 m class ground-based facilities and may offer a promising route to understanding the physical nature of the brightest $z \gtrsim 6$ galaxies.

ACKNOWLEDGEMENTS

We thank the referee for useful comments. We are grateful to Dawn Erb, Martin Haehnelt, Juna Kollmeier, Andrei Mesinger and Alice Shapley for enlightening conversations. DPS acknowledges support from the National Science Foundation through the grant AST-1410155. JR acknowledges support from the European Research Council (ERC) starting grant CALENDS and the Marie Curie Career Integration Grant 294074. SC, JG and AW acknowledge support from the ERC via an Advanced Grant under grant agreement no. 321323 – NEOGAL. The results are partially based on observations made with ESO telescopes at the La Silla Paranal Observatory under programme 092.A-0630 and the W. M. Keck Observatory. This work was partially supported by a NASA Keck PI Data Award, administered by the NASA Exoplanet Science Institute. Data presented herein were obtained at the W. M. Keck Observatory from telescope time allocated to the National Aeronautics and Space Administration through the agency's scientific partnership with the California Institute of Technology and the University of California. The Observatory was made possible by the generous financial support of the W. M. Keck Foundation. We acknowledge the very significant cultural role that the summit of Mauna Kea has always had within the indigenous Hawaiian community. We are most fortunate to have the opportunity to conduct observations from this mountain.

REFERENCES

Bayliss M. B., Rigby J. R., Sharon K., Wuyts E., Florian M., Gladders M. D., Johnson T., Oguri M., 2014, ApJ, 790, 144
Bolton J. S., Haehnelt M. G., 2013, MNRAS, 429, 1695
Bouwens R. J. et al., 2015, ApJ, 803, A34
Bowler R. A. A. et al., 2014, MNRAS, preprint (arXiv:1411.2976)
Bradley L. D. et al., 2014, ApJ, 792, 76
Bruzual G., Charlot S., 2003, MNRAS, 344, 1000
Caruana J., Bunker A. J., Wilkins S. M., Stanway E. R., Lacy M., Jarvis M. J., Lorenzoni S., Hickey S., 2012, MNRAS, 427, 3055
Caruana J., Bunker A. J., Wilkins S. M., Stanway E. R., Lorenzoni S., Jarvis M. J., Ebert H., 2014, MNRAS, 443, 2831
Chabrier G., 2003, PASP, 115, 763
Charlot S., Fall S. M., 2000, ApJ, 539, 718

Charlot S., Longhetti M., 2001, MNRAS, 323, 887
Christensen L. et al., 2012, MNRAS, 427, 1953
Curtis-Lake E. et al., 2012, MNRAS, 422, 1425
da Cunha E., Charlot S., Elbaz D., 2008, MNRAS, 388, 1595
Dijkstra M., Mesinger A., Wyithe J. S. B., 2011, MNRAS, 414, 2139
Dijkstra M., Wyithe S., Haiman Z., Mesinger A., Pentericci L., 2014, MNRAS, 440, 3309
Dunlop J. et al., 2013, MNRAS, 432, 3520
Ellis R. S. et al., 2013, ApJ, 763, L7
Erb D. K., Pettini M., Shapley A. E., Steidel C. C., Law D. R., Reddy N. A., 2010, ApJ, 719, 1168
Ferland G. J. et al., 2013, Rev. Mex. Astron. Astrofis., 49, 137
Finkelstein S. L. et al., 2013, Nature, 502, 524
Fontana A. et al., 2010, ApJ, 725, L205
Hainline K. N., Shapley A. E., Kornei K. A., Pettini M., Buckley-Geer E., Allam S. S., Tucker D. L., 2009, ApJ, 701, 52
Hashimoto T., Ouchi M., Shimasaku K., Ono Y., Nakajima K., Rauch M., Lee J., Okamura S., 2013, ApJ, 765, 70
Iye M. et al., 2006, Nature, 443, 186
James B. L. et al., 2014, MNRAS, 440, 1794
Jensen H., Laursen P., Mellema G., Iliev I. T., Sommer-Larsen J., Shapiro P. R., 2013, MNRAS, 428, 1366
Labbé I. et al., 2013, ApJ, 777, 19
McLean I. S. et al., 2012, in McLean I. S., Ramsay S. L., Takami H., eds, Proc. SPIE Conf. Ser. Vol. 8446, Ground-based and Airborne Instrumentation for Astronomy IV. SPIE, Bellingham, p. 84460J
McLinden E. M. et al., 2011, ApJ, 730, 136
McLure R. J. et al., 2013, MNRAS, 432, 2696
McQuinn M., Hernquist L., Zaldarriaga M., Dutta S., 2007, MNRAS, 381, 75
Mesinger A., Furlanetto S. R., 2008, MNRAS, 386, 1990
Mesinger A., Aykutalp A., Vanzella E., Pentericci L., Ferrara A., Dijkstra M., 2015, MNRAS, 446, 566
Oke J. B., Gunn J. E., 1983, ApJ, 266, 713
Ono Y. et al., 2012, ApJ, 744, 83
Ouchi M. et al., 2009, ApJ, 706, 1136
Ouchi M. et al., 2010, ApJ, 723, 869
Pacifici C., Charlot S., Blaizot J., Brinchmann J., 2012, MNRAS, 421, 2002
Pentericci L. et al., 2011, ApJ, 743, 132
Pentericci L. et al., 2014, ApJ, 793, 113
Richard J., Kneib J.-P., Ebeling H., Stark D. P., Egami E., Fiedler A. K., 2011, MNRAS, 414, L31
Robertson B. E., Ellis R. S., Dunlop J. S., McLure R. J., Stark D. P., 2010, Nature, 468, 49
Robertson B. E. et al., 2013, ApJ, 768, 71
Rodríguez Espinosa J. M. et al., 2014, MNRAS, 444, L68
Schenker M. A., Stark D. P., Ellis R. S., Robertson B. E., Dunlop J. S., McLure R. J., Kneib J.-P., Richard J., 2012, ApJ, 744, 179
Schenker M. A. et al., 2013a, ApJ, 768, 196
Schenker M. A., Ellis R. S., Konidaris N. P., Stark D. P., 2013b, ApJ, 777, 67
Schenker M. A., Ellis R. S., Konidaris N. P., Stark D. P., 2014, ApJ, 795, 20
Shapley A. E., Steidel C. C., Pettini M., Adelberger K. L., 2003, ApJ, 588, 65
Smit R. et al., 2014, ApJ, 784, 58
Smit R. et al., 2015, ApJ, 801, 122
Sobacchi E., Mesinger A., 2014, MNRAS, 440, 1662
Stark D. P., Ellis R. S., Chiu K., Ouchi M., Bunker A., 2010, MNRAS, 408, 1628
Stark D. P., Ellis R. S., Ouchi M., 2011, ApJ, 728, L2
Stark D. P. et al., 2014, MNRAS, 445, 3200
Steidel C. C., Erb D. K., Shapley A. E., Pettini M., Reddy N., Bogosavljević M., Rudie G. C., Rakic O., 2010, ApJ, 717, 289
Tapken C., Appenzeller I., Noll S., Richling S., Heidt J., Meinköhn E., Mehlert D., 2007, A&A, 467, 63
Tilvi V. et al., 2014, ApJ, 794, 5
Treu T., Schmidt K. B., Trenti M., Bradley L. D., Stiavelli M., 2013, ApJ, 775, L29
Vanzella E. et al., 2011, ApJ, 730, L35
Vanzella E. et al., 2014, A&A, 569, A78
Vernet J. et al., 2011, A&A, 536, A105
Zitrin A. et al., 2012, ApJ, 747, L9

This paper has been typeset from a TEX/LATEX file prepared by the author.